Magnetic phase transition in CoO under high pressure: A challenge for LSDA+*U*

Wenxu Zhang,[1,2] Klaus Koepernik,[2] Manuel Richter,[2] and Helmut Eschrig[2]
[1]*State Key Laboratory of Electronic Thin Films and Integrated Devices, University of Electronic Science and Technology of China, Chengdu 610054, People's Republic of China*
[2]*IFW Dresden, P.O. Box 270016, D-01171 Dresden, Germany*
(Received 12 January 2009; published 29 April 2009)

The high-spin low-spin transition under pressure in CoO is investigated by the local spin-density approximation plus onsite Coulomb correlation (LSDA+*U*) approach. The magnetic moment collapse is found to be caused by a competition between the ligand field and the intra-atomic exchange. The interplay of the interactions leads to a reduction in the symmetry below that of the antiferromagnetic order. This symmetry breaking causes a considerable reduction in the predicted moment-collapse transition pressure. For the multivalley functional of the LSDA+*U* approach it is crucial to consider initial conditions of self-consistency of sufficiently low symmetry. In particular, if an imposed symmetry would enforce a metallic solution for *U* of the order of the bandwidth, the commonly used symmetry breaking just by initial spin polarization may not be sufficient.

DOI: 10.1103/PhysRevB.79.155123 PACS number(s): 71.30.+h, 71.15.Mb, 71.27.+a, 75.20.Hr

I. INTRODUCTION

The behavior of transition-metal monoxides has attracted a lot of experimental and theoretical interest over the past decades. Under ambient conditions they are Mott insulators of charge transfer type,[1] and due to their simple rocksalt ($B1$) derived crystal structure they became reference cases for theoretical treatment of electronically strongly correlated systems, in particular of their magnetic interactions.[2] In recent time, phase diagrams of transition-metal monoxides under ultrahigh pressure became another important issue due to their relevance in earth science.[3] In Ref. 2, the local spin density approximation plus onsite Coulomb correlation (LSDA+*U*) approach[4] of density-functional theory (DFT) is suggested as a refinement of the presented tight-binding study of the magnetic couplings of the late 3*d* transition-metal monoxides.

Of these, MnO is the simplest at least under ambient pressure in that it has a filled majority and an unfilled minority 3*d* shell. In a systematic DFT study[5] employing LSDA+*U* and a number of related approaches to the correlation problem, a moment collapse $S=\frac{5}{2}\rightarrow\frac{1}{2}$ was predicted at low temperature and high pressure in correspondence with previous interpretation of room-temperature x-ray emission spectra (XES).[6,7] A further investigation[8] revealed an interesting breakdown of Hund's first rule at the transition in the still localized Mn *d* shell. In room-temperature diffraction experiments[9] and resistivity measurements[10] a structural insulator-to-insulator transition was found at 90 GPa followed by a Mott insulator-to-metal transition at 105 GPa.

Compared to MnO, CoO may be expected to be more complex due to a partial occupation of the Co-3*d* minority spin subshell by two electrons in addition to the filled majority subshell. At ambient pressure the room-temperature $B1$ structure distorts tetragonally with a slight superimposed rhombohedral distortion[11,12] at (or close to) and below the Néel temperature $T_N=290$ K. The observed magnetic order is essentially antiferromagnetic of type II (AFM-II) with magnetic wave vector $(\frac{1}{2},\frac{1}{2},\frac{1}{2})$, consistent with a rhombohedral distortion, but a superimposed slight tilt with AFM-I wave vector (0,0,1) was found in Ref. 12. The tetragonal distortion, known for at least 40 years, has early on given rise to speculations about its origin which could possibly be orbital order between second neighbor Co t_{2g} orbitals in octahedral anionic coordination[13] independent of the magnetic order. The magnetic tilt then could be induced. Inversely, the rhombohedral distortion could be induced by the basic AFM-II magnetic order. This scenario gets support from the recent finding[14] that T_N rises above room temperature at about 2 GPa pressure with no detectable tetragonal distortion of the cubic phase at room temperature. Three more structural room-temperature phase transitions of CoO were detected at higher hydrostatic pressure:[15,16] a cubic to rhombohedral transition at 43 GPa, a rhombohedral to rhombohedral transition at about 90 GPa, and a rhombohedral back to cubic transition at about 120 GPa. Resistivity measurements[17] revealed a drop in room-temperature resistivity by 8 orders of magnitude between 40 and 60 GPa, but at low temperature the material seemed to remain semiconducting above 100 GPa. A further less dramatic drop in room-temperature resistivity was observed at 90 GPa, and above 130 GPa the sample eventually became metallic down to at least 20 K. Room-temperature XES (Ref. 6) indicates a magnetic moment collapse $S=\frac{3}{2}\rightarrow\frac{1}{2}$ by quantitative analysis of the intensity (and position) of a satellite line of the ($3p$-$1s$) emission which is assumed proportional to the local moment by $3d$-$3p$ exchange interaction. When increasing the pressure from ambient the high-spin (HS) state was observed up to the highest applied pressure of 140 GPa. Laser heating of the sample at this pressure to release accumulated anisotropic stresses brought it into the low-spin (LS) state where it stayed down to about 97 GPa on pressure release. At 97 GPa the high-spin state reappeared. The collapse was proposed to be of $t_{2g}^5e_g^2\rightarrow t_{2g}^6e_g^1$ nature. The findings so far about the pressure phase diagram are summarized in Fig. 1.

In the present work we concentrate on the XES data since the resistivity data are expected to be largely influenced by shallow impurity levels in the gap. In particular at the cubic

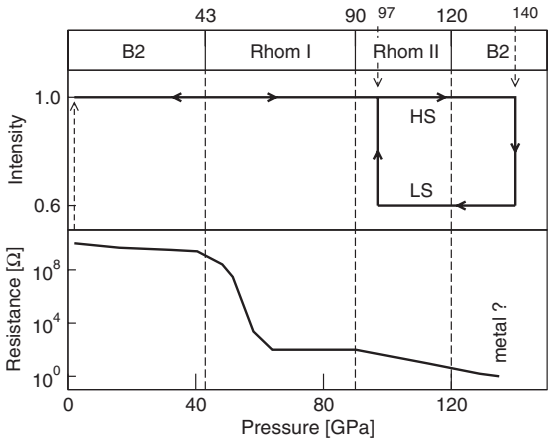

FIG. 1. Room-temperature structure (Refs. 14–16), AFM ordered moment (Ref. 6), and electrical resistance (Ref. 17) under pressure as summarized from recent experiments. Intensity means the satellite intensity of XES in arbitrary units. Magnetic order at room temperature sets in at about 2 GPa.

to rhombohedral transition around 40 GPa a dramatic increase in such levels (for instance due to twin boundaries) is to be expected, enhancing the conductivity. Therefore, we do not relate the measured resistivity data to the behavior of the intrinsic gap.

The magnetic collapse in transition-metal monoxides under pressure was first discussed within the Stoner scenario by employing the LSDA or generalized gradient approximation (GGA) approaches of DFT.[3,18] For CoO a transition into an itinerant nonmagnetic (NM) metallic state was found at 88 GPa in Ref. 3, while for the other monoxides it was found at much higher pressure. These calculations did not take the correlation-localized character of the transition-metal 3*d* shell into account, which is suggested by an excitation gap (for CoO) as large as[19] 2.5 ± 0.3 eV or, as very recently determined,[20] 2.6 eV.

In the present paper, the LSDA+*U* functional is used to investigate the magnetic moment collapse of CoO under high pressure. The results reveal that a competition between the ligand-field splitting of the Co-3*d* levels and the onsite exchange interaction drive the system into low-symmetry low-spin phase. The HS LS transition is indeed obtained to be of $t_{2g}^5 e_g^2 \rightarrow t_{2g}^6 e_g^1$ character. Not unexpectedly the transition is insulator to insulator as was found for MnO. This contradicts the experimentally observed resistivity data, which however are not obtained down to lowest temperatures. Besides the incomplete experimental information a tendency of LSDA+*U* to favor insulating solutions may contribute to this discrepancy.

In Sec. II the computational details are explained. Section III shortly reconsiders the LSDA findings for the sake of comparison, while Sec. IV presents and discusses our LSDA+*U* results in more detail. Conclusions are drawn in Sec. V.

II. COMPUTATIONAL PARAMETERS

The calculations are performed in the rhombohedral (trigonal) unit cell (space group $R\bar{3}m$) of the AFM-II magnetic structure, with the lattice geometry and atomic positions corresponding to the undistorted cubic *B*1 lattice (Fig. 2). It is expected that a small rhombohedral distortion induced by the magnetic structure will not influence the anticipated results. With respect to the rhombohedral coordinate axes, the two antiferromagnetically coupled Co atoms occupy the Wyckoff positions 1*a* (0,0,0) and 1*b* $(\frac{1}{2},\frac{1}{2},\frac{1}{2})$, respectively, while the O atoms occupy the 2*c* $(\frac{1}{4},\frac{1}{4},\frac{1}{4})$ position. The calculations are performed with the full-potential local-orbital code[21] in the version FPLO8.50–32 (Ref. 22) with the default basis settings. All calculations are done within the scalar relativistic approximation. We used the "atomic limit" (AL) flavor of the double counting term in the LSDA+*U* calculations. The projector on the correlated orbitals was defined such that the trace of the occupation number matrices represents the 3*d* gross occupation. The choice of the double counting term is motivated by a recent analysis of the LSDA+*U* functionals,[23] which suggests that the AL functional is better suited for the description of localized shells. The LSDA exchange-correlation functional is parameterized according to Perdew-Wang 92.[24] The number of $\boldsymbol{k}$ points in the Brillouin zone is set to 20^3 in order to get a reasonably high accuracy of the computed total energies.

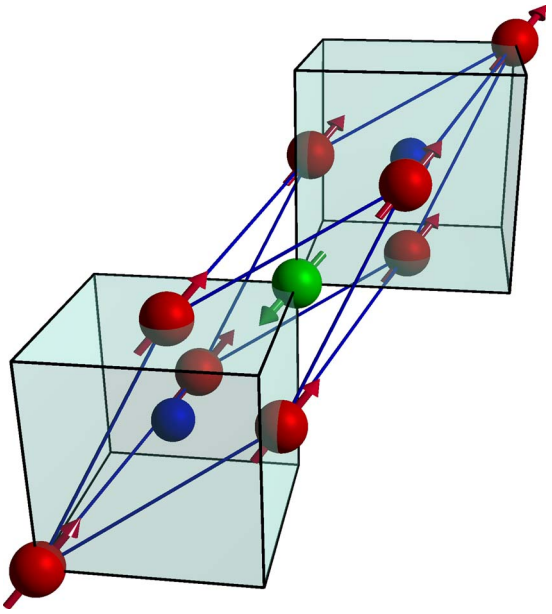

FIG. 2. (Color online) The conventional unit cell of CoO in the antiferromagnetic AFM-II state. The spin alignment of the Co atoms is indicated by the arrows. The rhombohedral *z* axis is identical with the 111 direction in the cubic rocksalt crystal.

III. LSDA RESULTS

As a starting point of the discussion we shortly report the LSDA results for CoO. We obtain an equilibrium volume of 117.5 atomic units per formula unit (a.u./f.u.), which is by 9 p.c. smaller than the experimental volume of 129.5 a.u./f.u.[11] This deviation is well within the usual error limits of the LSDA.

In Fig. 3 the orbital projected densities of states (PDOSs) of the Co-3*d* and O-2*p* orbitals are presented. Note that the

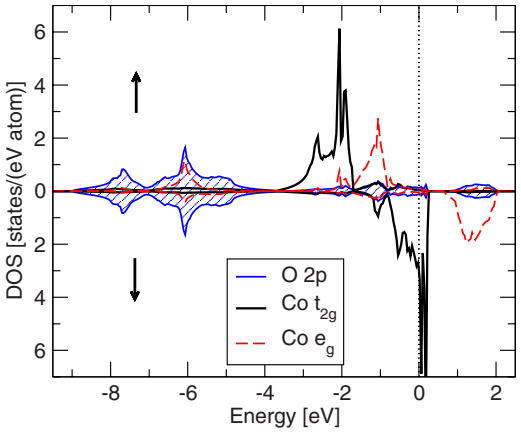

FIG. 3. (Color online) LSDA-PDOS of the Co-3*d* and O-2*p* states. The 3*d* states are resolved into the irreducible representations of the approximate cubic site symmetry. The shaded area corresponds to the O-2*p* states. The Fermi level is marked by a dashed vertical line. Arrows indicate the spin channel.

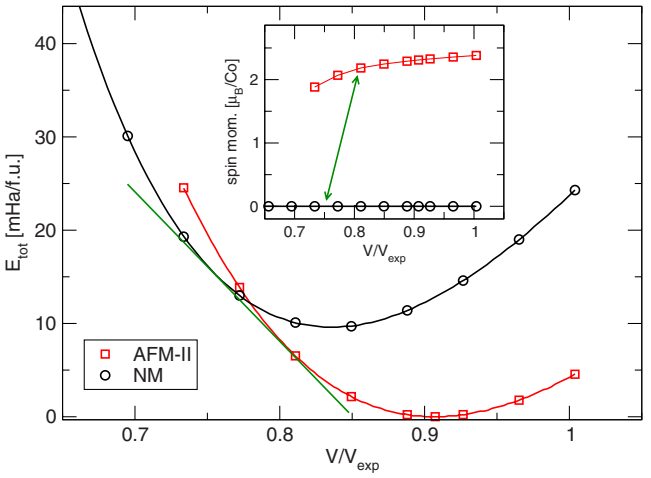

FIG. 4. (Color online) Energy and spin moment versus volume for the NM and AFM-II state of CoO in LSDA. The reference volume is the experimental volume $V_{exp}=129.5$ a.u./f.u. The arrow in the inset corresponds to the common tangent in the main figure.

rhombohedral symmetry, forced upon the system by the AFM-II magnetic order, splits the cubic t_{2g} manifold into a one-dimensional irreducible representation (irrep) a_g and into a two-dimensional irrep e_g'. The cubic e_g manifold is unaltered; however the two resulting e_g irreps may mix to form two other e_g irreps. The mixing is determined by the interactions of the system of which the octahedral ligand field is the leading interaction at the Co sites yielding an approximate cubic site symmetry. If we discuss the cubic irreps in the following it is meant in the sense of the approximate cubic site symmetry. The PDOS shown corresponds to the LSDA equilibrium volume. The e_g and t_{2g} ligand-field separation is clearly visible and can be estimated to be $\Delta_{lf} \approx 1.3$ eV (averaged about the spin directions).

The exchange splitting of about $\Delta_x \approx 2.2$ eV, which corresponds to a spin moment of about 2.3 μ_B, indicates a Co-3*d* Stoner exchange parameter $I \approx 0.95$ eV. All Co-3*d* majority states are occupied, in accordance with Hund's first rule. The O-2*p* states are located $\Delta_{pd} \approx 4$ eV below the Co-3*d* states. For each Co-3*d* orbital character a bandwidth $W \approx 1.3$ eV can be read off of Fig. 3.

Under hydrostatic pressure, the local spin moment of Co decreases monotonically to eventually vanish after a first-order transition into the nonmagnetic state at a volume of about 80 p.c. relative to the experimental volume. The transition pressure amounts to $p_c \approx 37$ GPa. Figure 4 shows the energy and spin moment versus volume curves. Our findings basically reproduce the LSDA results by Cohen *et al.*,[3] who attributed the collapse of the magnetic moment to the Stoner criterion no longer being satisfied.

As discussed by Terakura *et al.*,[25] the partially filled minority spin t_{2g} states give rise to the metallic behavior in the LSDA model. The exchange and ligand-field splitting can produce an insulating state in MnO and NiO but not in FeO and CoO. Terakura *et al.*[25] proposed that a large orbital moment in these latter two compounds could induce a band gap because the spin-orbit interaction will lead to a population imbalance among the three t_{2g} derived orbitals such that two of them become occupied.

An electronic structure calculation by Norman,[26] where spin-orbit coupling and orbital polarization corrections were included, confirmed this proposal. However, the resulting total magnetic moment is too large and the band gap is too small. If the orbital moment was corrected to its experimental value (about 50 p.c. of the calculated value), it would be to small to open the gap. So, Norman[26] concluded that more sophisticated orbital polarization functionals were desired in order to correctly describe the insulating state in CoO.

IV. LSDA+*U* RESULTS

Clearly, LSDA does not correctly describe the electronic state of CoO under ambient pressure, which is calling for an LSDA+*U* approach. In a Hubbard model scenario, the importance of correlation is measured by U/W, where U denotes the isotropic part of the screened onsite Coulomb repulsion of a pair of electrons in localized orbitals (here the 3*d* orbitals of Co) and W denotes the bandwidth of the relevant bands. Under pressure, W usually increases while U might decrease due to an increase in the screening efficiency. Nevertheless, the gross failure of LSDA ($U=0$) to predict an insulator at ambient pressure implies sizable onsite correlations, which will survive to a certain extend under pressure. Moreover, there are other aspects of correlations, such as anisotropic exchange (Hund's second rule), which are poorly described by LSDA and might become important. Also the mechanism of the transition and the physical picture of the concomitant moment collapse depend on the treatment of the correlation effects.

Different viewpoints on the behavior of CoO under pressure were taken in the literature. As discussed, Ref. 3 and citations therein treated a HS-NM transition by LSDA as a competition between band energy and exchange energy according to a Stoner scenario. On the other hand, as proposed by Ohnishi,[27] the ligand-field splitting is another candidate for producing a HS-LS transition in some transition-metal complexes. As mentioned in the previous section and shown

in Sec. IV A, the parameters Δ_{pd} and U on the one hand and W, I (or J), and Δ_{lf} on the other are of the same scale and hence may compete in determining the electronic state. Thus it is necessary to incorporate all of them (or equivalent ones[2]) into a model in order to uncover the physics underlying the materials behavior. Very recently,[28] a two-orbital model Hamiltonian involving U, J, and Δ_{lf} has been solved, showing that all of these parameters strongly influence the HS-LS transition. In this work, we will use the LSDA+U approach, which contains some of the strong correlation aspects, most notably the occupation-dependent level splitting (upper and lower Hubbard bands) and anisotropic exchange.

A. Electronic structure of the ground state

LSDA+U changes several ground-state properties of CoO as compared to LSDA (U=0). Most notably and not unexpectedly the electronic ground state becomes insulating with a gap of several eV, depending on the value of U. Furthermore, the theoretical equilibrium mechanical properties change, although not very drastically.

We performed volume variations in the AFM-II HS state for various values of U. The Hund's rule J, which enters the LSDA+U model was kept fixed to J=1 eV$\approx I$. The main action of J is the reduction in the effective occupation-dependent level splitting $[\pm(U-J)/2]$. Thus, for this term the choice of a different value of J is merely a redefinition of the appropriate U. The second action of J is to produce anisotropic exchange, which is expected to be of minor importance in the HS state. Hence, we do not expect qualitative changes in the results under reasonable variation in J.

The resulting energy versus volume curves have been fitted to Birch's equation of state[29] (EOS),

$$E(V) = E_0 + \frac{9}{8}B_0V_0\left[\left(\frac{V_0}{V}\right)^{2/3} - 1\right]^2 + \frac{9}{16}B_0V_0(B_0' - 4) \times \left[\left(\frac{V_0}{V}\right)^{2/3} - 1\right]^3, \quad (1)$$

in order to obtain values for the equilibrium volume V_0, the bulk modulus B_0, and its pressure derivative B_0'. In order to assess the quality of the fit the size of the volume interval entering the fit has been varied and we conclude that B_0 is reliable within a few percent, while B_0' has an uncertainty of up to 10%. A summary of the results is shown in Fig. 5 and Table I. One first notices that even for high values of U the experimental equilibrium volume (V_0=1) is not obtained. The electronic gap on the other hand is reproduced with a value of $U\approx$5 eV. The bulk modulus decreases with increasing U but like the volume never reaches the experimental value. It is understandable that underestimation of the volume correlates with overestimation of the bulk modulus. The pressure derivative B_0' is independent of U; however the large uncertainty of this value puts the results into the correct range. (Values of B_0'=3.8 can easily be obtained by using a different EOS model.) All together, it seems reasonable to choose U=5 eV for further calculations since this choice will reproduce the value of the experimental gap, while the mechanical properties are relatively insensitive.

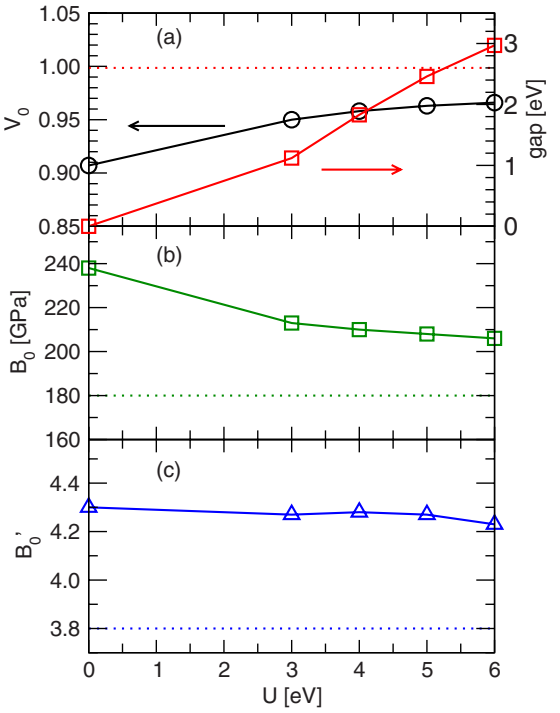

FIG. 5. (Color online) The dependence of ground-state properties on the value of U. The black curve (circles) in panel (a) shows the equilibrium volume relative to the experimental volume. The curve with the square symbol (red) in panel (a) shows the gap. The dotted line indicates the experimental value for the gap. Panels (b) and (c) show the bulk modulus B_0 and its pressure derivative B_0'. Again the dotted lines denote the experimental values.

The site projected spin magnetic moment of Co increases from $\mu_{\mathrm{Co}}=2.31\mu_B$ for U=0 to $\mu_{\mathrm{Co}}=2.80\mu_B$ for U=6 eV, which is consistent with the increasing degree of localization when the correlation strength grows. The full moment corresponding to the spin S=3/2 is not obtained for two reasons. On the one hand the projected site moments are not very well defined quantities and on the other the hybridization with oxygen reduces the moment compared to the formal HS integer value.

The PDOSs of the Co-3d and O-2p states for the high-spin AFM-II state are shown in Fig. 6. This picture corre-

TABLE I. LSDA+U ground-state properties of CoO with varying values of U. The experimental data (exp) (Refs. 11, 16, 19, and 20) are given in the last row. The spin magnetic moment μ_{Co} is defined by projection onto the Cocentered basis orbitals.

U (eV)	$\frac{V_0}{V_{\mathrm{exp}}}$	B_0 (GPa)	B_0'	Band gap (eV)	μ_{Co} (μ_B)
0	0.907	238	4.30	0	2.31
3	0.950	213	4.27	1.11	2.60
4	0.958	210	4.28	1.82	2.67
5	0.963	208	4.27	2.45	2.74
6	0.966	206	4.23	2.97	2.80
exp	1.0	180	3.8	2.6	

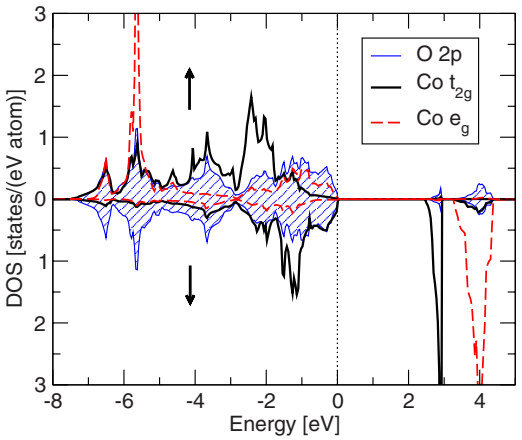

FIG. 6. (Color online) The Co-3d and O-2p PDOS at the equilibrium volume for $U=5$ eV. The Co-3d DOS is decomposed according to the approximate cubic site symmetry. The O-2p DOS is indicated by the shaded area. Arrows indicate the spin channel. The top of the valence band is marked by a dashed line at 0 eV.

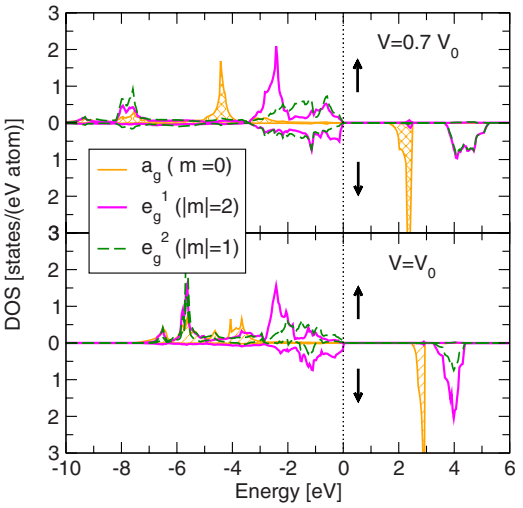

FIG. 7. (Color online) The Co-3d PDOS of the high-spin phase at the theoretical equilibrium volume and at 70% of this volume. The $V=V_0$ panel shows the same data as Fig. 6 but now resolved into the irreducible representations of the AFM-II rhombohedral symmetry. Arrows indicate the spin channel. The shaded area indicates the a_g contribution. The near degeneracy of the unoccupied $e_g^{1,2}$ states in the upper panel is incidental.

sponds to the theoretical equilibrium volume for $U=5$ eV. The unoccupied minority t_{2g} and e_g orbitals around 3–4 eV are mainly formed by Co-3d states. The smallness of the hybridization with the O-2p state allows to estimate the ligand-field splitting from these states, which as for the LSDA calculations amounts to $\Delta_{\mathrm{lf}} \approx 1.3$ eV. Closer comparison with the PDOS obtained within LSDA (Fig. 3) shows, however, remarkable differences. In LSDA, the O-2p states are situated well below the Co-3d states (by $\Delta_{pd} \approx 4$ eV), while in LSDA+U the downshift of the occupied Co-3d states brings them into the energy region of the O-2p states, which increases hybridization. Thus, the 3d states are spread over a wide energy range from −7 eV up to the gap. We observe that the majority states between −1 and 0 eV are to a large part of oxygen 2p character, which shows the charge transfer character of this compound. In the minority channel Co-3d states have a larger contribution to the total DOS, which allows them to contribute to the excitations. Experimentally, detailed resonant photoemission spectroscopy (RPES) measurements[30] from 2p and 3p core levels confirm the charge transfer character of CoO. In Ref. 31 a single impurity Anderson model has been used to simulate experimental spectroscopy data. From this the charge transfer energy Δ_{pd} was determined to be 4.0 eV. Our value of $U=5$ eV (which reproduces the experimental gap) and the $\Delta_{pd} \approx 4$ eV $\approx U$ from our LSDA results fulfill the condition for a Mott insulator of charge transfer character (case AB of Ref. 1).

B. Magnetic transitions in LSDA+U

In the following, majority and minority occupations are discussed in which case the site projected quantities are meant. The compound is considered in the AFM-II magnetic state such that the second Co atom has the same but opposite spin moment.

The main action of LSDA+U is the shift of levels or bands depending on their occupation. There are however symmetry restrictions on the possible splittings. E.g., if a band complex has a certain multidimensional irreducible representation at the Γ point and if this representation does not appear more than once in this band complex then the degeneracy of the representation at Γ cannot be lifted by LSDA+U. In other words, there will not appear a gap within this irrep. It is assumed in this discussion that the calculation is carried out with or results in a certain symmetry. The first case comes about by user-enforced symmetry restrictions, which help to speed up and to stabilize calculations, while the second case may arise due to stable attractors in the iterative landscape, which prevent the relaxation into less symmetric solutions.

For example, the gap-prohibiting conditions are fulfilled for the irreps of the 3d states in cubic site symmetry. Figure 6 shows that the minority t_{2g} states are partially occupied, with an unoccupied part situated at ≈3 eV above the Fermi level. This part contains roughly one hole. Of course this kind of splitting of the t_{2g} representation would be impossible in a perfect cubic symmetry. However, as discussed above the true symmetry of the calculation is rhombohedral, which allows for this kind of splitting. The seeming contradiction to the above-mentioned rule comes from the labeling according to the cubic irreps used in the decomposition of the PDOS.

In the lower panel of Fig. 7 we show the PDOS for the same calculation as in Fig. 6 but now within the irreps of the true symmetry of the AFM-II phase. It becomes clear that the before-mentioned split-off minority t_{2g} states belong to the a_g symmetry. The unoccupied "cubic" e_g levels however are composed of both e_g^1 and e_g^2. Thus, for these states the cubic e_g classification seems to be quite reasonable. In general the specific shape of the e_g states cannot be assessed from symmetry arguments due to the possible mixing of both e_g com-

ponents. Moreover, the majority and minority e_g irreps need not be the same mixture. In the following the occupations of the $3d$ shell are discussed in both the cubic and the rhombohedral projections. Note that the occupation number matrix need not be and is in general not diagonal in either of the two corresponding bases. Hence, the two resulting interpretations reflect different aspect of the system: the cubic setting emphasizes the octahedral ligand field, while the rhombohedral setting emphasizes the aspects of the symmetry, induced by the antiferromagnetic order.

In the monoxide, Co is formally in a $3d^7$ configuration, which gives rise to $S=3/2$ for the high-spin solution. Although the actual occupation numbers (and spin moments) do not have integer values it is helpful to discuss the system in terms of an isolated atomic shell, mainly because the character of the bands is quite clearly assignable to the atomic species, which makes the integer occupation number picture valid in the band (Hilbert) space.

When discussing the possible magnetic solutions we have to take into account all relevant interactions. There are three leading interactions: the ligand field, exhibiting an octahedral symmetry to a certain extend, the exchange interaction following the rhombohedral symmetry with the threefold axis along the cubic 111 direction (the antiferromagnetic wave vector), and the correlation energy $(U-J)$. The isotropic part of the exchange interaction $E_x^{\mathrm{iso}}=-\frac{1}{4}IM^2$ favors the high-spin solution (Hund's first rule). This remains unchanged under pressure as long as the ligand field remains small enough. The unoccupied minority states in the upper panel of Fig. 7 clearly show an increased ligand-field splitting $\Delta_{\mathrm{lf}}\approx 2$ eV under pressure. This value is comparable to the exchange splitting, bringing low-spin solutions into the game. Possible antiferromagnetic LS solutions can be constructed by simple arguments. The U-J term favors insulating solutions over metallic solutions as long as it is large enough compared to the ligand field. Hund's first rule will prefer larger spins, which makes $S=1/2$ more likely than $S=0$ solutions. A $3d^7$ configuration can have $S=3/2$ (HS), $S=1/2$ (LS), and $S=0$ (NM). Note that in this particular case the $S=0$ solution does not have integer occupation, due to the odd number of $3d$ electrons. This state is, however, the ground state at very high pressures and therefore included in the discussion. The following patterns can be created (and are actually found in the calculations):

(1) insulating HS: the majority $3d$ shell is filled with five electrons and the two minority electrons go into e_g states, preferably in a representation derived from the cubic t_{2g} symmetry. The unoccupied states have a_g and almost cubic e_g symmetry.

(2) Insulating LS rhombohedral: one electron has to go from the majority into the minority states. Due to the dimensionality of the rhombohedral irreps there is only one insulating LS pattern with four majority electrons: the two e_g manifolds are filled and the a_g is empty. In the minority channel the ligand field prefers the cubic t_{2g}-derived states to be filled (a_g and e_g') while the cubic e_g is empty. This solution is penalized due to the violation of the ligand-field level order in the majority channel, where a_g (which derives from t_{2g}) is empty. In fact this solution stays energetically above the HS solution up to at least 50% of the experimental volume.

(3) Metallic LS $\mu=1\mu_B$: this is almost the same pattern as in the insulating LS case, but the majority spin occupation does not violate the ligand-field order. The t_{2g} derived states are full and the remaining electron is sitting in the e_g states, making it a metal. The actual calculation gives a slightly different pattern: the majority channel is filled quite evenly, while the occupied minority states resemble cubic t_{2g} character. In terms of rhombohedral irreps the half-filled majority e_g states belong to the $|m|=1$ crystal harmonics of the rhombohedral orientation, while the unoccupied minority e_g states are formed in equal parts by the $|m|=1$ and $|m|=2$ harmonics. The resulting spin density is formed to a large amount by the $|m|=2$ orbital, which extends into the plane perpendicular to the AFM wave vector.

(4) Metallic LS $\mu=1.2\mu_B$: energetically nearly degenerate with the previous solution is another one, which has a 20% higher moment. This cannot easily be predicted by simple arguments and was found in the course of calculation. The difference is that a small amount of the cubic e_g-like majority electrons flips their spin, which results in the increase in the moment. In terms of rhombohedral irreps the half-filled majority e_g states are now mostly of $|m|=2$ character, while the unoccupied minority e_g states are mostly of $|m|=1$ character. This results in a spin density of strong $|m|=1$ signature, pointing into the direction of the AFM wave vector

(5) Metallic NM: this is the solution, which was considered as the high-pressure candidate in previous studies.[3,32] It is strongly penalized by the U-J term which favors insulators and by the exchange energy, which favors higher-spin moments. Not unexpectedly, it turns out to not be the ground state up to very high pressures. In contrast to the LSDA calculations of Sec. III, where this was the only thinkable competitor, it is the least likely medium pressure ground state in LSDA+U. This might actually be a shortcoming of the static LSDA+U method in which U is a parameter. One would expect that the correct value of U for this theory would renormalize to a small value, when finally a transition into a metallic state takes place. Attempts to calculate U from constraint LSDA calculations for MnO[8] have shown to yield a quite pressure-independent value of U, which is an obstacle in predicting the transition into the metallic state correctly.

The list of solution patterns discussed so far exhausts all possibilities compatible with a $3d^7$ configuration with integer occupations (with the exception of case 5), a rhombohedral symmetry, and the leading interactions. We have shown that all low-spin solutions in the list above have an energy penalty. In order to find a solution with lower energy one has to lift the symmetry restrictions. This will produce one-dimensional representations out of the two e_g representations. In this way one can produce an insulating solution, which follows the ligand-field implied level order. We have found two solutions of this type:

(a) insulating LS monoclinic 1: the first solution has a monoclinic axis, which is formed by one of the C_2 axes of the rhombohedral symmetry perpendicular to the AFM wave vector. (There are three equivalent orientations of this axis with respect to the lattice.) The resulting spin density shown in Fig. 8(a) points to a direction perpendicular to the C_2 axis and to the AFM wave vector.

(b) Insulating LS monoclinic 2: this is a variation on the previous solution and both are in fact nearly energetically

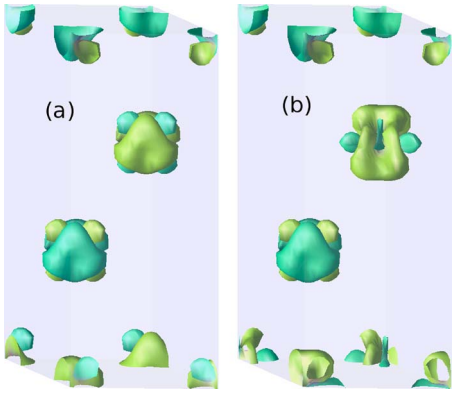

FIG. 8. (Color online) Spin-density isosurfaces of the two low-symmetry insulating LS solutions. The left panel shows solution 1, which is symmetric with respect to simultaneous exchange of the two Co atoms and spin directions. The color code denotes positive and negative densities. The right panel shows the solution, where the Co atoms have inequivalent spin densities. Both solutions have monoclinic symmetry.

degenerate. Both Co atoms still have essentially $S=1/2$ and both spin densities are pointing into similar directions [Fig. 8(b)]. However, the shape of the spin densities of the two atoms differs.

Figure 9 shows the 3d PDOS of the lower symmetric monoclinic solution (case b above) projected both on the approximate cubic and (now) approximate rhombohedral representations. While the decomposition into rhombohedral representations does not reveal much information the cubic decomposition clearly shows an approximate $t_{2g}^6 e_g^1$ character.

In Fig. 10 we have summarized the total energy versus volume curves for the solutions discussed above. We have left out the nearly degenerate solutions for clarity. It is apparent that the inclusion of the low-symmetry solution reduces the resulting transition pressure significantly. The other solutions do not compete up to a pressure of ≈ 300 GPa and can be ignored. We obtain a first-order transition from the HS into the monoclinic LS state with a transition pressure amounting to $p_c=128$ GPa, which corresponds to 70% of the experimental volume. The resulting volume collapse is about 3.5%. At the transition the spin moment jumps from its HS value of $2.66\mu_B$ to the LS value of $0.84\mu_B$. Under further compression the gap in the LS solution decreases and the system becomes metallic at $p_{c,\mathrm{met}} \approx 200$ GPa ($0.62V_{\mathrm{exp}}$). The magnetic moment after the insulator-to-metal transition is still quite high, $\mu=0.82\mu_B$, and eventually vanishes at higher pressures. For comparison the HS to metallic LS transition would occur at 197 GPa; the HS to nonmagnetic transition would occur at 210 GPa. Of course, the transition pressure is strongly U dependent (see Table II), and we merely discuss trends here.

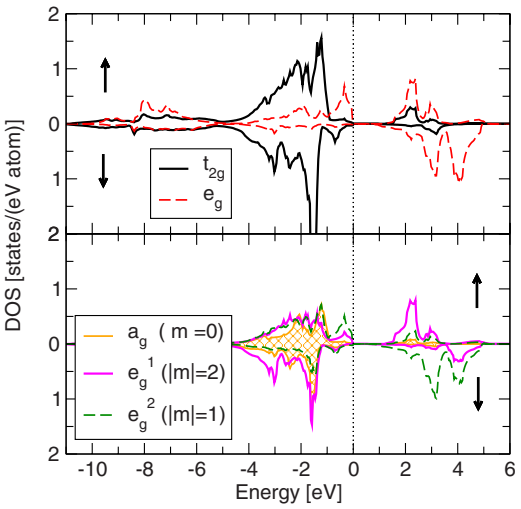

FIG. 9. (Color online) The Co-3d PDOS of the low-symmetric insulating low-spin phase (monoclinic case b) at the transition point ($V=0.7V_{\mathrm{exp}}$). The upper panel shows the decomposition into the cubic representation while the lower panel shows the projection onto the rhombohedral representations. Arrows indicate the spin channel, while the color code and shading follows the ones used in the previous figures.

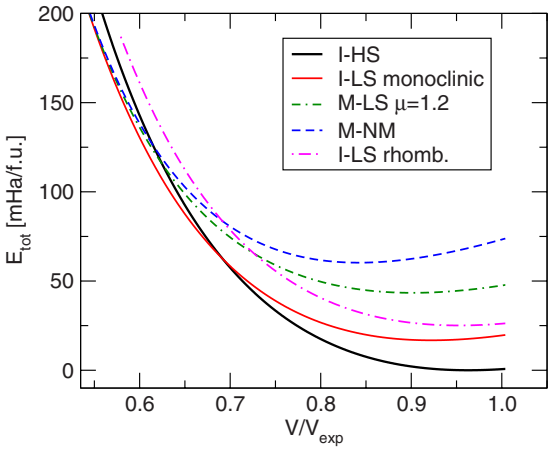

FIG. 10. (Color online) Energy versus volume for the different magnetic solutions of CoO in LSDA+U. The reference volume is the experimental volume. The legend refers to the list of solutions discussed in the text. I and M refer to insulating and metallic, respectively. The two insulating LS solutions differ by their symmetry. The one denoted rhomb is the one that violates the ligand-field level order, while the one denoted monoclinic is the low-symmetry solution, which is in agreement with the energetics of the leading interactions.

The shape of the spin densities as shown in Fig. 8 implies a possible instability toward a nonrhombohedral distortion. We did not try to make a full relaxation of the system for all volumes, which would be rather costly. Still we confirmed for one particular volume that the rhombohedral lattice symmetry is not the most stable solution. The resulting distortion was small, and from this we argue that the transition pressure

TABLE II. HS to insulating low-symmetric LS solution transition pressure versus U. The pressure for $U=0$ (LSDA) refers to the transition into the nonmagnetic state since the LS solution collapses for small U. However the transition pressures for the different solutions converge to each other with decreasing U.

U [eV]	0	3	4	5	6
p_c [GPa]	37	92	111	128	145

would not be changed drastically if the relaxation is taken fully into account.

C. Reasons for the magnetic transition

Let us summarize the energetic arguments, which make the HS-LS transition observed in the LSDA+U calculations plausible. The specific filling of the 3d shell with seven electrons leads to a partial occupation of the cubic t_{2g} minority states in the high-spin phase. The unoccupied t_{2g}-derived state belongs to the a_g irrep of the AFM-II rhombohedral symmetry. This splitting is stabilized by the leading isotropic term of the LSDA+U interaction proportional to U-J.

Under pressure, the ligand field Δ_{lf} becomes stronger due to an increased hybridization with the ligand oxygen 2p-states and according to our estimate from Fig. 7 it reaches the size of $2J \approx 2$ eV at around $V_c = 0.7 V_{\mathrm{exp}}$. In the LS solution one electron has to flip its spin, and that roughly costs an energy of 2J. J, being to a large extent an intra-atomic quantity, can be expected to be much less sensitive to volume reduction than the ligand-field splitting. This simple argument supports the transition point being located at around V_c. The nature of the irreps in the AFM-II symmetry forces such a LS solution to be metallic in the majority channel, which adds a penalty stemming from the same isotropic U term discussed above for the metallic occupation number fluctuations. Hence, for such a metallic solution the transition takes place at a higher pressure, where the ligand field also compensates this penalty. If a symmetry lowering is allowed, the system can obey the level order implied by the ligand field and it will stay insulating. Besides the main interactions discussed so far there is the anisotropic exchange, which tends to increase the mutual electron separation by preferring certain orbital occupation patterns and which played a vital role in the transition into the LS phase in MnO.[8] In CoO it is not of such central importance, which certainly can be attributed to the different filling of the 3d shell. Nevertheless, its presence can be inferred from the shape of the spin densities (Fig. 8), which shows a complex internal antiferromagnetic structuring at each separate atom (however less pronounced than for MnO).

D. Comparison with previous results

In a recent publication[32] GGA+U calculations on CoO were reported. The authors find a transition pressure of only 80 GPa for a transition from the high-spin to the nonmagnetic state. They used $U=7.1$ eV but also showed the decrease in the transition pressure with decreasing U. The LSDA/GGA+U method is implementation dependent, and hence the appropriate value of U for certain quantities is not the same for different methods. The pressures published in Ref. 32 are, however, much lower than ours for all U. More importantly they discuss the transition into the nonmagnetic phase, which on the grounds of very general arguments, should happen at a higher pressure than the transition into a LS phase discussed in the present work. The authors further claim consistency of their findings with the previous work of Cohen *et al.*,[3] which reported $p_c = 88$ GPa in GGA ($U=0$). We expect that GGA+U with U values of several eV gives significantly higher transition pressures than GGA due to the stabilization of insulating solutions. Wdowik and Legut[32] reported a reduction in the transition pressure from 80 GPa for $U=7.1$ eV to 45 GPa for $U=4.1$ eV, which does not seem to be consistent with the results of Cohen *et al.*[3] for $U=0$. In the inset of Fig. 2 in Ref. 32 the enthalpies for the HS and NM solutions are shown. The enthalpies must be continuous curves, which cross each other at the transition. The resulting discontinuity of the derivative with respect to pressure is related to the volume collapse. The enthalpy curves as shown in this figure do not cross at the pressure of 80 GPa, and we conclude that the true transition pressure of their approach (crossing point of the curves) is much higher.

V. CONCLUSIONS

In our calculation, LSDA+U was employed with U given *ad hoc*. We choose $U=5$ eV in order to reproduce the experimental band gap at ambient pressure. U was kept constant with respect to pressure since comparison of total energies with different values of U is not justified within LSDA+U. Although, the occupation fluctuations will be enhanced under high pressure, which likely leads to a change in U, the pressure dependence of U is anyway not readily available. Our main result, the character of the HS-LS transition, is not changed under moderate variation in U. However, the transition pressure is U dependent.

The inability of LSDA+U to correctly predict the final insulator-to-metal transition is a major shortcoming of this method. Still, our study sheds some light on the possible type of the low-spin phase and on the mechanism of the moment-collapse transition. The resulting low-symmetry $S=1/2$ solution implies a lattice distortion connected to the emergence of a low-spin phase. The precise nature of the low-spin phase cannot with certainty be deduced from our study since a multitude of other orbital arrangements is thinkable. Nevertheless, the breaking of the symmetry in order to avoid a metallic solution is the central feature of the physics discussed in this work. It is a result of the main interaction introduced by LSDA+U and therefore a quite general behavior.

ACKNOWLEDGMENTS

Discussions with D. Kasinathan, U. Nitzsche, and I. Chaplygin are gratefully acknowledged. W.Z. got financial support from the DAAD and partially from the Youth Foundation of UESTC.

[1] J. Zaanen, G. A. Sawatzky, and J. W. Allen, Phys. Rev. Lett. **55**, 418 (1985).

[2] W. A. Harrison, Phys. Rev. B **76**, 054417 (2007).

[3] R. E. Cohen, I. I. Mazin, and D. G. Isaak, Science **275**, 654

(1997).
[4] V. I. Anisimov, F. Aryasetiawan, and A. I. Lichtenstein, J. Phys. Condens. Matter **9**, 767 (1997).
[5] D. Kasinathan *et al.*, Phys. Rev. B **74**, 195110 (2006).
[6] J.-P. Rueff, A. Mattila, J. Badro, G. Vankó, and A. Shukla, J. Phys. Condens. Matter **17**, S717 (2005).
[7] A. Mattila, J.-P. Rueff, J. Badro, G. Vankó, and A. Shukla, Phys. Rev. Lett. **98**, 196404 (2007).
[8] D. Kasinathan, K. Koepernik, and W. E. Pickett, New. J. Phys. **9**, 235 (2007).
[9] C. S. Yoo *et al.*, Phys. Rev. Lett. **94**, 115502 (2005).
[10] J. R. Patterson, C. M. Aracne, D. D. Jackson, V. Malba, S. T. Weir, P. A. Baker, and Y. K. Vohra, Phys. Rev. B **69**, 220101(R) (2004).
[11] W. Jauch, M. Reehuis, H. J. Bleif, F. Kubanek, and P. Pattison, Phys. Rev. B **64**, 052102 (2001).
[12] K. Tomiyasu, T. Inami, and N. Ikeda, Phys. Rev. B **70**, 184411 (2004).
[13] K. I. Kugel' and D. I. Khomskii, Sov. Phys. Usp. **25**, 231 (1982).
[14] Y. Ding, Y. Ren, P. Chow, J. Zhang, S. C. Vogel, B. Winkler, J. Xu, Y. Zhao, and H.-K. Mao, Phys. Rev. B **74**, 144101 (2006).
[15] Y. Noguchi, T. Atou, T. Kondo, T. Yagi, and Y. Syono, Jpn. J. Appl. Phys. **38**, L7 (1999).
[16] Q. Guo, H.-K. Mao, J. Hu, J. Shu, and R. J. Hemley, J. Phys. Condens. Matter **14**, 11369 (2002).
[17] T. Atou, M. Kawasaki, and S. Nakajima, Jpn. J. Appl. Phys. **43**, L1281 (2004).
[18] D. G. Isaak, R. E. Cohen, M. J. Mehl, and D. J. Singh, Phys. Rev. B **47**, 7720 (1993).
[19] J. van Elp, J. L. Wieland, H. Eskes, P. Kuiper, G. A. Sawatzky, F. M. F. de Groot, and T. S. Turner, Phys. Rev. B **44**, 6090 (1991).
[20] E. Z. Kurmaev, R. G. Wilks, A. Moewes, L. D. Finkelstein, S. N. Shamin, and J. Kuneš, Phys. Rev. B **77**, 165127 (2008).
[21] K. Koepernik and H. Eschrig, Phys. Rev. B **59**, 1743 (1999).
[22] http://www.fplo.de, Tech. Rep. (2008).
[23] E. R. Ylvisaker, W. E. Pickett, and K. Koepernik, Phys. Rev. B **79**, 035103 (2009).
[24] J. P. Perdew and Y. Wang, Phys. Rev. B **45**, 13244 (1992).
[25] K. Terakura, A. R. Williams, T. Oguchi, and J. Kübler, Phys. Rev. Lett. **52**, 1830 (1984).
[26] M. R. Norman, Phys. Rev. Lett. **64**, 1162 (1990).
[27] S. Ohnishi, Phys. Earth Planet. Inter. **17**, 130 (1978).
[28] P. Werner and A. J. Millis, Phys. Rev. Lett. **99**, 126405 (2007).
[29] F. Birch, J. Geophys. Res. **83**, 1257 (1978).
[30] Z.-X. Shen, C. K. Shih, O. Jepsen, W. E. Spicer, I. Lindau, and J. W. Allen, Phys. Rev. Lett. **64**, 2442 (1990).
[31] M. Magnuson, S. M. Butorin, J.-H. Guo, and J. Nordgren, Phys. Rev. B **65**, 205106 (2002).
[32] U. D. Wdowik and D. Legut, J. Phys. Chem. Solids **69**, 1698 (2008).